



¹⁵N photo-CIDNP MAS NMR analysis of reaction centers of *Chloracidobacterium thermophilum*

Jeremias C. Zill¹ · Zhihui He² · Marcus Tank^{2,3} · Bryan H. Ferlez² · Daniel P. Canniffe² · Yigal Lahav^{4,5} · Peter Bellstedt⁶ · A. Alia^{1,7,8} · Igor Schapiro⁴ · John H. Golbeck^{2,9} · Donald A. Bryant^{2,10} · Jörg Matysik¹

Received: 5 February 2018 / Accepted: 23 March 2018 / Published online: 30 March 2018
© Springer Science+Business Media B.V., part of Springer Nature 2018

Abstract

Photochemically induced dynamic nuclear polarization (photo-CIDNP) has been observed in the homodimeric, type-1 photochemical reaction centers (RCs) of the acidobacterium, *Chloracidobacterium (Cab.) thermophilum*, by ¹⁵N magic-angle spinning (MAS) solid-state NMR under continuous white-light illumination. Three light-induced emissive (negative) signals are detected. In the RCs of *Cab. thermophilum*, three types of (bacterio)chlorophylls have previously been identified: bacteriochlorophyll *a* (BChl *a*), chlorophyll *a* (Chl *a*), and Zn-bacteriochlorophyll *a'* (Zn-BChl *a'*) (Tsukatani et al. in J Biol Chem 287:5720–5732, 2012). Based upon experimental and quantum chemical ¹⁵N NMR data, we assign the observed signals to a Chl *a* cofactor. We exclude Zn-BChl because of its measured spectroscopic properties. We conclude that Chl *a* is the primary electron acceptor, which implies that the primary donor is most likely Zn-BChl *a'*. Chl *a* and 8¹-OH Chl *a* have been shown to be the primary electron acceptors in green sulfur bacteria and heliobacteria, respectively, and thus a Chl *a* molecule serves this role in all known homodimeric type-1 RCs.

Keywords Chlorophototrophy · Reaction centers · *Chloracidobacterium thermophilum* · ¹⁵N-MAS NMR · Photo-CIDNP · Zn-BChl *a'*

Electronic supplementary material The online version of this article (<https://doi.org/10.1007/s11120-018-0504-1>) contains supplementary material, which is available to authorized users.

✉ Jörg Matysik
joerg.matysik@uni-leipzig.de

¹ Institute of Analytical Chemistry, University of Leipzig, Johannisallee 29, 04103 Leipzig, Germany

² Department of Biochemistry and Molecular Biology, The Pennsylvania State University, University Park, PA 16802, USA

³ Department of Biological Sciences, Tokyo Metropolitan University, 1-1 Minami-Osawa, Hachioji-shi, Tokyo 192-0397, Japan

⁴ Fritz Haber Center of Molecular Dynamics, Institute of Chemistry, The Hebrew University of Jerusalem, 91904 Jerusalem, Israel

⁵ Migal-Galilee Research Institute, S. Industrial Zone, 12100 Kiryat Shmona, Israel

Introduction

Chloracidobacterium (Cab.) thermophilum was discovered in 2007 in microbial mats of hot springs in Yellowstone National Park, WY, USA (Bryant et al. 2007). It is the first chlorophototrophic species in the phylum of *Acidobacteria*,

⁶ Institute of Organic and Macromolecular Chemistry, Friedrich-Schiller-Universität Jena, Humboldtstraße 10, 07743 Jena, Germany

⁷ Leiden Institute of Chemistry, University of Leiden, Einsteinweg 55, P.O. Box 9502, 2300 RA Leiden, The Netherlands

⁸ Institute of Medical Physics and Biophysics, University of Leipzig, Härtelstr. 16-18, 04107 Leipzig, Germany

⁹ Department of Chemistry, The Pennsylvania State University, University Park, PA 16802, USA

¹⁰ Department of Chemistry and Biochemistry, Montana State University, Bozeman, MT 59717, USA

and at the time of its discovery, it extended the number of phyla containing chlorophototrophic bacteria to six. Recently, a phototrophic species named *Gemmatimonas phototrophica* strain AP64^T from a seventh bacterial phylum (Gemmatimonadetes) has been described (Zeng et al. 2014). *Cab. thermophilum* and “*Ca. Thermochlorobacter aerophilum*” are the only known aerobic chlorophototrophs that have type-1 homodimeric reaction centers (RC) (Bryant and Frigaard 2006; Liu et al. 2012; Tsukatani et al. 2012; Tank and Bryant 2015a, b; Tank et al. 2017). RCs are able to convert light energy into chemical energy and are, therefore, the key to the photochemical process of chlorophyll-based phototrophy (i.e., chlorophototrophy) (Tsukatani et al. 2012). There are two groups of photosynthetic RCs: type-1 RCs that utilize iron–sulfur clusters as terminal electron acceptor, and type-2 RCs that contain quinone molecules for this purpose (Golbeck 2003). Photosystem I of cyanobacteria and higher plants is a heterodimeric, type-1 RC. Homodimeric type-1 RCs are also found in the anaerobic heliobacteria and green sulfur bacteria. Previously, this was explained by the sensitivity of the Fe₄–S₄ clusters towards oxygen (Overmann 2001; Madigan 2001). However, it was later found that, unless it is illuminated, *Chlorobaculum (Cba.) tepidum* is tolerant to oxygen, suggesting that reactive oxygen species causes the damage (Li et al. 2009). The RCs of purple bacteria, including aerobic anoxygenic phototrophic bacteria and *G. phototrophica* AP64^T, and the filamentous anoxygenic phototrophic bacteria contain type-2 RCs. Photosystem II of plants and cyanobacteria are also type-2 RCs (Golbeck 2003; Oh-oka 2007). All type-2 RCs have heterodimeric cores and utilize (bacterio)-pheophytin molecules as the primary electron acceptor.

(Bacterio)-chlorophylls [(B-)Chls] act in various processes in chlorophototrophic bacteria. In addition to the function of light harvesting and the associated transfer of excitation energy, they act as primary electron donor and primary electron acceptor in photosynthetic RCs. Based on a porphyrin structure, Chls and BChls comprise a central atom (usually a Mg²⁺ ion but sometimes Zn²⁺) and different substituents at the outer macrocycle carbons. Pheophytins, which do not coordinate to a central atom, act as primary electron acceptors in type-2 RCs. In the RC complex of *Cab. thermophilum*, reverse-phase high-performance liquid chromatography (RP-HPLC) revealed the presence of three different Chls: BChl *a*, Chl *a*, and Zn-BChl *a'* in a ratio of about 12.8:8.0:2.0 (Tsukatani et al. 2012). Zn-BChl *a'* was only found in the RC and was not present in chlorosomes, the light-harvesting antenna complexes of this organism, nor in the FMO antenna protein that only contained BChl *a* (Wen et al. 2011; Tsukatani et al. 2012). Zn-BChl *a'* was suggested to function as the primary electron donor (Tsukatani et al. 2012). In the literature, ¹H and ¹³C chemical shifts of Zn-BChl *a* have been reported (Kobayashi et al. 1998, 2016). In this work, ¹⁵N liquid-state NMR

data from this cofactor are presented to provide reference values for the ¹⁵N photo-CIDNP MAS NMR spectra.

The solid-state photo-CIDNP effect (Jeschke and Matysik 2003; Daviso et al. 2008a; Bode et al. 2013; Sosnovsky et al. 2016) provides selective access to information on the electron donor and the primary electron acceptor that form a spin-correlated radical pair. It allows the detection of electron transfer chain cofactors of isolated RCs, and it can be used to detect these cofactors at nanomolar concentrations in intact cells (Prakash et al. 2006; Janssen et al. 2010). The electronic ground-state structures of the electron donor and acceptor forming a spin-correlated radical pair is reflected in the observed chemical shifts. Electron spin densities can be deduced from the photo-CIDNP MAS NMR intensities. There are up to three mechanisms that occur in parallel and that contribute to the solid-state, photo-CIDNP effect: (1) three-spin mixing (TSM), generally yielding emissive signals; (2) differential decay (DD); and (3), if the lifetime of the donor triplet state is sufficiently long, differential relaxation (DR) giving enhanced absorptive signals (Jeschke 1998; McDermott et al. 1998; Polenova and McDermott 1999). Recently, the spin dynamical system has been re-interpreted in terms of level crossings and anti-crossings within an electron–electron–nuclear spin scheme (Sosnovsky et al. 2016).

The solid-state photo-CIDNP effect has already been observed in the RCs of nine species, including plants (Alia et al. 2004; Diller et al. 2005; Roy et al. 2007b; Janssen et al. 2010, 2012), bacteria (Zysmilich and McDermott 1994; Schulten et al. 2002; Prakash et al. 2005, 2006; Diller et al. 2008; Roy et al. 2007a), and Chromista (Zill 2017a). An overview of these species is presented in Fig. 1. In addition, the effect has been observed for the blue-light photoreceptor phototropin LOV1-C57S (Thamarath et al. 2010) from the green alga *Chlamydomonas reinhardtii*. There are seven bacterial phyla with chlorophototrophic members (Tank et al. 2017; Thiel et al. 2017). The effect has not yet been observed in the phyla *Acidobacteria*, *Chloroflexi*, and *Gemmatimonadetes*. In the present work, the solid-state photo-CIDNP effect was studied in the membranes of *Cab. thermophilum* from the phylum *Acidobacteria*. The fact that the solid-state photo-CIDNP effect has been observed in all taxonomic kingdoms and in a large variety of phyla implies that the effect is an inherent property of natural photosystems (Matysik et al. 2009) and that it probably reflects conserved features of light-induced charge separation in reaction centers with important functional relevance (Céspedes-Camacho and Matysik 2014).

pipetting and were pooled in an ultracentrifugation tube. The membrane fraction was diluted with five volumes of PBS to reduce the sucrose concentration of the sample in two subsequent washing steps. The pooled membranes were centrifuged at $250,000\times g$ for 2 h. The supernatants were discarded and the membrane pellets were resuspended in ~ 25 mL PBS and centrifuged again at $220,000\times g$ for 2 h. In a final step the membrane pellet was resuspended in a minimal volume of ~ 1.5 mL PBS isolation buffer. The absorption spectrum of these chlorosome-depleted membranes showed a strong enrichment of the characteristic absorption features of FMO and RCs of *Cab. thermophilum*, which have a maximum at 809 nm and a shoulder at 823 nm (Fig. S1B). Washed membranes were stored at 4 °C in the dark until they were required for analysis.

For photo-CIDNP MAS NMR experiments, the volume was reduced using Centricon Plus-20 centrifugal filter devices (Amicon®, Millipore Corporation, Bedford, USA, 30 kDa molecular weight cutoff) performing centrifugation for 12 min at $4000\times g$. Membranes containing RCs were reduced by adding 1 M sodium dithionite solution up to a final concentration of 100 mM in an oxygen-free atmosphere.

MAS NMR measurements

Solid-state NMR measurements were performed with an Avance-III 400-MHz NMR spectrometer equipped with a 4-mm MAS probe. The sample was loaded in a 4-mm sapphire rotor and inserted into the MAS probe. Freezing slowly helped to obtain homogeneous sample distribution against the rotor wall (Fischer et al. 1992). The light and dark spectra were collected with a Hahn-echo pulse sequence and two-pulse phase modulation (TPPM) proton decoupling (Bennett et al. 1995). ^{15}N -MAS NMR spectra were obtained at a temperature of 250 K under continuous illumination with white light (1000 W xenon arc lamp) (Matysik et al. 2000). The rotational frequency for MAS was 8 kHz and the cycle delay was 0.5, 4, or 12 s. Artificial line broadening of 40 Hz was applied prior to Fourier transformation. All the ^{15}N -NMR spectra were referenced using the amino NH_2 response of histidine $\cdot\text{HCl}$ at 49.09 ppm.

Preparation of ^{15}N -labeled Zn-BChl *a*

Cultures of *Rhodobacter (Rba.) sphaeroides* were grown phototrophically using ^{15}N -ammonium sulfate (95%) as the sole nitrogen source in anoxic M22+ medium. Zn-BChl *a* was prepared from Mg-BChl *a* by slight modification of a previously described method (Chen et al. 2016). Briefly, one volume of extracted ^{15}N -labeled Mg-BChl *a* in methanol was mixed with excess zinc acetate, 50 mM sodium ascorbate, and six volumes of glacial acetic acid.

The mixture was incubated at 90 °C for 1 h. After centrifugation at $10,000\times g$ for 5 min, the supernatant was transferred to a clean tube and dried in a vacuum concentrator at 30 °C. The dried pigments were dissolved in methanol and purified by reversed-phase HPLC on an Agilent 1100 HPLC system (Agilent Technologies) with a semi-preparative Discovery C18 column (10 mm \times 25 cm) (Supelco, Sigma-Aldrich) using a modified method (Van Heukelem et al. 1994). Solvents A and B were 80:20 (v/v) methanol–500 mM ammonium acetate and 80:20 (v/v) methanol–acetone, respectively. Pigments were eluted at 3.5 mL min^{-1} with a linear gradient of 92–93% solvent B over 10 min, increasing to 100% to wash the column. Elution of Zn-BChl *a* was monitored at 770 nm. Approximately 9 mg of ^{15}N -labeled Mg-BChl *a* was extracted from the cells of a 200-mL culture of *Rba. sphaeroides*, and the final yield of ^{15}N -labeled Zn-BChl *a* was approximately 1 mg. The identity of the compound was established by its absorption spectrum (Fig. 2), which had maxima at 355 and 763 nm (Wakao et al. 1996). Mass spectrometry showed that the purified ^{15}N -Zn-BChl *a* had m/z of 955.5 (M^+) (Fig. S2) compared to Mg-BChl *a* (calculated mass = 910.6) and ^{14}N -Zn-BChl *a* (calculated mass = 950.5) (Tsukatani et al. 2012; Kobayashi et al. 2006). As expected, the mass confirmed the replacement of Mg by Zn (+ 39.9) and the substitution of the four ^{14}N pyrrole nitrogens with ^{15}N (+ 4). Furthermore, the purified ^{15}N -Zn-BChl *a* exhibited the characteristic isotopic abundance pattern for compounds containing Zn (Tsukatani et al. 2012). After the NMR experiments, infrared (Fig. S3) and Raman spectra (Fig. S4) were also obtained.

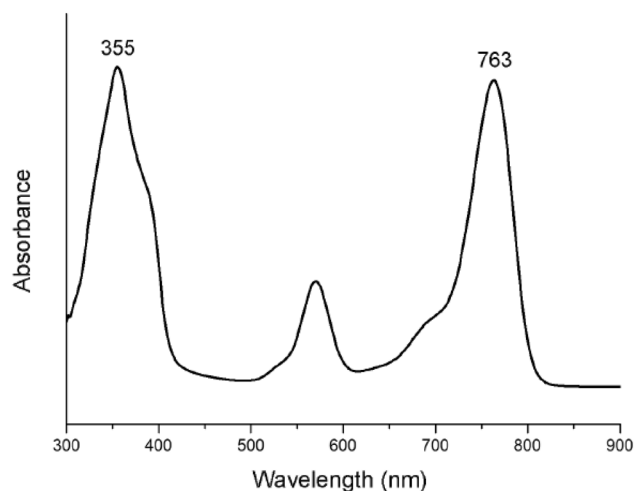


Fig. 2 The absorption spectrum of Zn-BChl *a* showing the characteristic maxima at 355 and 763 nm

Solution-state NMR measurements

For the solution-state NMR measurements, ^{15}N -Zn-BChl *a* (~3 mg) was dissolved in d^8 -tetrahydrofuran (THF- d^8). The ^1H -NMR spectrum and the ^{15}N - ^1H -HMQC were measured at 600 MHz using a cryoProbe. The ^{15}N -NMR spectrum and the ^{13}C -APT spectrum were acquired in the same solvent at 500 MHz using a Prodigy-BBO probehead. ^1H and ^{13}C spectra were referenced to TMS. ^{15}N spectra were referenced to liquid ammonia using a solution of 90% formamide in DMSO as external standard.

Quantum chemical calculations of ^{15}N -chemical shifts

The Zn-BChl *a* geometry was optimized at the B3LYP/6-31G* level of theory (Becke 1993; Rassolov et al. 2001), including the Grimme's dispersion correction (Grimme et al. 2011) and the SMD implicit solvent model (Marenich et al. 2009) with THF as the solvent. In order to reduce complexity, the phytol tail was replaced with a methyl group. In addition, we have added an explicit THF molecule to saturate the

axial coordination of zinc. There are two options for THF ligation, called “ α ” and “ β ” as shown in Fig. 3. In the case of α ligation, the THF molecule and the C-17¹ atom are on opposite faces of the tetrapyrrole macrocycle (Fig. 3 top), while for β ligation, the THF molecule is on the same side of the macrocycle as the C-17¹ atom (Fig. 3 bottom).

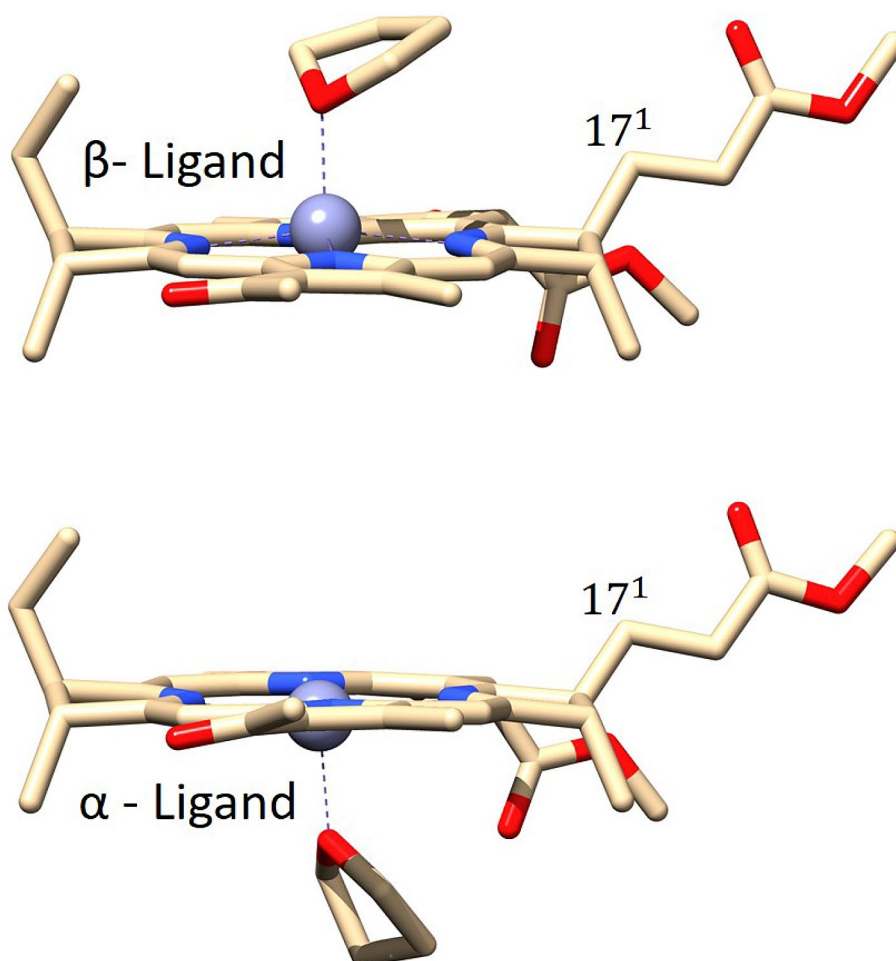
The isotropic shielding tensors were calculated using B3LYP/6-31G* level of theory and the gauge-invariant atomic orbitals (GIAO) method (Ruud et al. 1993), and chemical shifts were taken with respect to the isotropic shielding of ammonia 254.97 ppm, which was calculated at the same level of theory. All calculations were performed using the Gaussian 09 software package (Frisch et al. 2009).

Results and discussion

^{15}N photo-CIDNP MAS NMR spectra from *Cab. thermophilum*

Figure 4 shows the ^{15}N -MAS NMR spectra of uniformly ^{15}N -labeled membranes of *Cab. thermophilum*. All spectra

Fig. 3 Zn-BChl *a* with one explicit THF molecule in α and β positions. Top THF molecule at the α position. The THF and atom C17¹ are in opposite faces of the tetrapyrrole macrocycle. Bottom THF molecule at the β position. The THF and atom C17¹ are at the same faces of the tetrapyrrole macrocycle



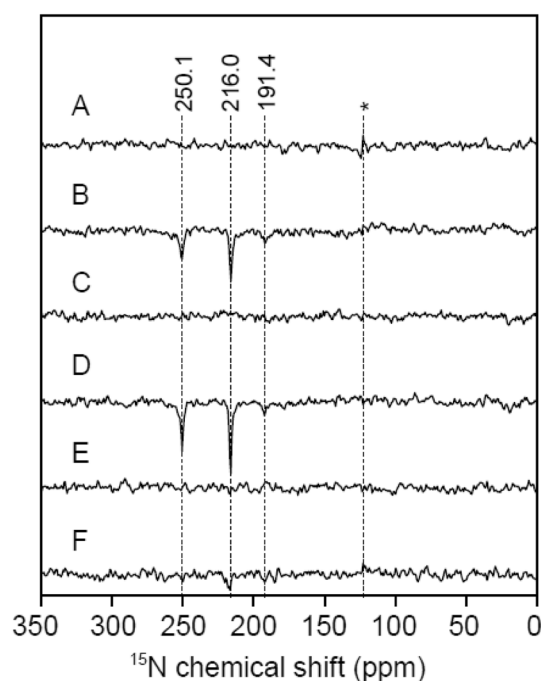


Fig. 4 ^{15}N -photo-CIDNP effect observed on *Cab. thermophilum*: **a** dark, cycle delay = 12 s, 16,300 scans; **b** light, cycle delay = 12 s, 16,300 scans; **c** dark, cycle delay = 4 s, 45,000 scans; **d** light, cycle delay = 4 s, 45,000 scans; **e** dark, cycle delay = 0.5 s, 345,000 scans; **f** light, cycle delay = 0.5 s, 345,000 scans, *spectrometer signal

(A–F) were recorded for about 2 days with different cycle delays. Spectra A, C, and E were collected in the dark, and no signal is observed. Due to the relatively low concentration of the sample, no signal from the protein is observed. Spectra B, D, and F were measured under continuous illumination with white light. Spectra A and B were collected with a cycle delay of 12 s (16,300 scans). Spectra C and D were measured with a cycle delay of 4 s (45,000 scans), and a cycle delay of 0.5 s (345,000 scans) was used for spectra E and F. The strongest light-induced signals are observed in spectra B and D. In spectrum F only a signal at 216.0 ppm can be observed. This is due to a too short cycle delay of 0.5 s, which does not allow for sufficient relaxation. Hence, the optimal cycle delay is around 4 s. All signals are light-induced and emissive (negative). In the ^{15}N -photo-CIDNP MAS NMR spectrum, no splitting of the signals is observed as in the special pair of *Rba. sphaeroides* (Daviso et al. 2008b). Hence, we can conclude that the observed set of signals occur either from a perfect dimer or a monomeric donor (i.e., in a strongly and functionally asymmetric dimeric donor). To obtain a maximal light-induced signal, a detailed view of the sum of spectra B and D of Fig. 4 is provided in Fig. S5. Upon illumination, three signals emerge in the aromatic region at 250.1, 216.0, and 191.4 ppm. The observation of these three signals implies that the signals occur from only one cofactor, which is either the electron

donor or the primary electron acceptor. It would be possible that both donor and acceptor would be of the same type of cofactor; however, one would not expect that they would show perfectly overlapping chemical shifts.

In the RCs of *Cab. thermophilum*, three types of cofactors have been identified (Chl *a*, BChl *a*, and Zn-BChl *a'*) (Tsukatani et al. 2012). Careful repetition of reversed-phase HPLC and reversed-phase HPLC–MS analysis again revealed only the same three pigments, and no 8¹-OH Chl *a* was detected. ^{15}N -chemical shifts of Chl *a* and Zn-BChl *a* was prepared to obtain ^{15}N -chemical shifts under solution-state conditions.

Solution-state NMR spectra from Zn-BChl *a*

Figure S6 shows the $^1\text{H}^{15}\text{N}$ -HMQC spectrum of Zn-BChl *a*. Analysis of this spectrum confirmed the assignment of the three protons H-5, H-10, and H-20 of the porphyrin ring (for numbering, see Fig. S7). Each of these protons is coupled via three bonds to an sp^3 - and an sp^2 -hybridized N atom. It is a characteristic feature of BChl *a* and, hence, also Zn-BChl *a'*, that each pyrrole nitrogen is coupled to a different number of protons. The resonance at 180.1 ppm is coupled to one proton only and must, therefore, be induced from the nitrogen of ring-III. Nitrogen N-I arises at 178.1 ppm which is confirmed by the ^3J -coupling to two protons at 9.11 ppm (H-5) and 8.52 ppm (H-20). The signal at 261.5 ppm is coupled to three protons. Hence, these resonances can be assigned to N-IV. In addition, a weak fourth crosspeak occurs due to the ^4J -coupling to H-13² at 6.05 ppm. This nitrogen N-II resonates at 259.4 ppm. Table 1 summarizes the experimental ^{15}N assignments. The macrocycle of Zn-BChl *a* with 55 C-atoms and 74 protons shows overlapping of a number of signals and the assignment of the resonances of the phytol side chain remains incomplete. The structure is presented in Fig. S7.

An overview on the chemical shifts assigned to the ^{13}C and ^1H positions in comparison to literature data is provided in Tables 2 and 3, respectively. The assignment in this work is almost identical to the chemical shifts observed in the literature (Kobayashi et al. 1998, 2016). In addition to the known signals, four ^{13}C -resonances and two ^1H -resonances have been assigned for the first time. Hence, the signals of Zn-BChl *a* are assigned completely except for those associated with the phytol side chain.

Calculation of the ^{15}N -chemical shifts from Zn-BChl *a*

Figure S8 shows the optimized geometries of Zn-BChl *a* and Zn-BChl *a'* with one THF molecule as the fifth ligand at either the α or β positions. It was found that in the case of Zn-BChl *a*, the α -ligand is energetically preferable by $\sim 4.21 \text{ kJ mol}^{-1}$ ($\sim 0.0436 \text{ eV}$). However, in the case of

Table 1 Tentative assignment of the chemical shifts obtained by ^{15}N photo-CIDNP MAS NMR in comparison to other photo-CIDNP MAS NMR data and calculations

	^{15}N -chemical shift (ppm)			
	N-I	N-II	N-III	N-IV
BChl a^a	191.8	258.3	196.9	258.3
Chl a^b	186.0	206.0	189.4	247.0
Zn-BChl a^c	178.1	259.4	180.1	261.5
<i>Cab. thermophilum</i> ^d		216.0	191.4	250.1
Type-1 RC from				
<i>P. tricornutum</i> ^e	186.0	212.0	195.9	251.9
Spinach ^f	186.2	211.5	193.2	250.3
<i>Heliobacillus (H.) mobilis</i> ^g	188.4	216.2	195.5	248.6
Zn-BChl a α ligand ^h	179.6	259.2	179.8	265.3
Zn-BChl a β ligand ^h	180.7	261.8	179.2	261.3
Zn-BChl a implicit solvent ^h	180.7	268.1	179.1	260.0
Zn-BChl a gas phase ^h	179.9	262.7	177.5	259.1
Zn-BChl a' β ligand ^h	182.6	261.3	181.3	252.5
Zn-BChl a' α ligand ^h	183.8	261.9	180.5	254.5
Zn-BChl a' implicit solvent ^h	181.5	265.5	181.4	259.6
Zn-BChl a' gas phase ^h	181.0	263.1	177.7	254.9
Chl a α ligand ^h	185.9	207.0	189.1	245.6
Chl a β ligand ^h	187.0	207.1	187.6	243.6
Chl a implicit solvent ^h	184.9	203.3	186.0	235.1
Chl a gas phase ^h	184.5	202.9	184.5	232.7
R-8 ¹ -OH Chl a α ligand ^h	185.8	207.4	188.7	245.3
S-8 ¹ -OH Chl a α ligand ^h	185.8	210.3	189.1	244.9
R-8 ¹ -OH Chl a β ligand ^h	186.7	207.4	187.5	243.8
S-8 ¹ -OH Chl a β ligand ^h	186.6	210.3	187.9	243.5
R-8 ¹ -OH Chl a implicit solvent ^h	184.4	203.3	185.5	239.4
S-8 ¹ -OH Chl a implicit solvent ^h	184.4	206.3	185.9	239.1
R-8 ¹ -OH Chl a gas phase ^h	184.5	202.8	183.9	232.8
S-8 ¹ -OH Chl a gas phase ^h	184.6	206.0	184.5	232.3

^aMeasured in the solid state, data from Egorova-Zachernyuk et al. (2008)

^bMeasured in solution in acetone- d_6 , data from Boxer et al. (1974)

^cThis work, measured in solution in THF- d_8

^dThis work, photo-CIDNP MAS NMR

^eData from Zill (2017a) assigned to Chl a

^fData from Diller et al. (2007a), assigned to Chl a

^gData from Thamarath et al. (2012), assigned to 8¹(OH)-Chl a

^hThis work, theoretically calculated

Zn-BChl a' , the β -ligand is more stable by $\sim 3.15 \text{ kJ mol}^{-1}$ ($\sim 0.0327 \text{ eV}$). In addition, the two geometries of 8¹-OH Chl a were calculated (Fig. S9), showing that the *S* configuration is $\sim 3.52 \text{ kJ mol}^{-1}$ ($\sim 0.0365 \text{ eV}$) more stable than the *R* configuration.

Table 1 also compiles the theoretically calculated values. Clearly, the trends in the experimental data are well reproduced and Chl a and Zn-BChl a can be readily distinguished.

Table 2 Comparison of ^{13}C chemical shifts (ppm) of Zn-BChl a in different solvents

Carbon position	Zn-BChl a in THF d_8 (this work)	Zn-BChl a in acetone- d_6 (Kobayashi et al. 2016)
1	140.5	142.1
2	149.1	150.7
2 ¹	12.84	13.9
3	135.9	137.3
3 ¹	198.0	199.6
3 ²	33.1	33.4
4	148.8	149.8
5	98.2	98.9
6	166.6	168.6
7	47.2	47.7
7 ¹	22.6	23.0
8	54.8	55.0
8 ¹	29.8	–
8 ²	9.9	10.5
9	157.8	158.7
10	100.2	101.6
11	148.5	149.2
12	124.4	124.3
12 ¹	11.1	11.9
13	129.7	130.1
13 ¹	188.0	189.2
13 ²	64.56	65.2
13 ³	170.2	171.2
13 ⁴	51.4	–
14	158.9	160.0
15	108.5	109.5
16	152.6	153.1
17	49.7	50.1
17 ¹	29.5	–
17 ²	30.0	–
17 ³	172.3	173.3
18	48.4	49.0
18 ¹	22.5	23.0
19	165.6	167.8
20	95.1	96.4
P1	60.6	61.3
P2	118.5	119.2
P3	141.6	142.6
P3 ¹	20.0	16.1
P4	39.6	40.0

For numbering, see Fig. S7

P phytol side chain

The differences between the values of the four calculated forms of Zn-BChl a are too small to conclude the state of that molecule in THF solution. The calculations of the ^{15}N -chemical shifts of Zn-BChl a and Zn-BChl a' show that

Table 3 Comparison of ^1H chemical shifts (ppm) of Zn-BChl *a* in different solvents

Proton position	Zn-BChl <i>a</i> in THF d ⁸ (this work)	Zn-BChl <i>a</i> in acetone- d ⁶ (Kobayashi et al. 1998)
2 ¹	3.52	3.49
3 ²	3.08	3.09
5	9.11	8.95
7	4.34	4.30
7 ¹	1.80	1.77
8	4.10	4.07
8 ¹	2.41, 2.09	2.40, 2.09
8 ²	1.14	1.10
10	8.55	8.55
12 ¹	3.41	3.36
13 ²	6.05	6.02
13 ⁴	3.77	3.81
17	4.01	3.99
17 ¹	2.55, 2.32	2.50, 2.37
17 ²	2.41, 2.07	2.02
18	4.37	4.39
18 ¹	1.72	1.70
20	8.52	8.57
P1	4.48	4.38, 4.29
P2	5.20	5.06
P3 ¹	1.92	1.54
P4	1.61	–

For numbering, see Fig. S7

P phytol side chain

the chemical shift differences between the epimers are nearly identical and differ by only a few ppm. Furthermore, solely on the basis on ^{15}N NMR, it would also be difficult to distinguish Chl *a* and 8¹-OH Chl *a*.

Assignment of the ^{15}N -photo-CIDNP MAS NMR signals from *Cab. thermophilum*

Having obtained the ^{15}N -chemical shifts from Zn-BChl *a*, the sets of ^{15}N -chemical shifts are now available for all cofactors associated with the RCs of *Cab. thermophilum*. Table 1 provides an overview on the photo-CIDNP MAS NMR signals from *Cab. thermophilum* in comparison to solution-state NMR data for the pure cofactors. Furthermore, ^{15}N -photo-CIDNP MAS NMR data are presented for other RCs of plants (Diller et al. 2007a), bacteria (Thamarath et al. 2012), and Chromista (Zill 2017a), together with the ^{15}N -chemical shift calculations from Zn-BChl *a* and Zn-BChl *a'* as well as from Chl *a* and 8¹-OH Chl *a* determined in this study. On the basis of the chemical shift values obtained by experiments and calculations (summarized in Table 1), we can identify the (B)Chl cofactor that best

matches the three ^{15}N photo-CIDNP MAS NMR signals observed in *Cab. thermophilum* (Fig. S5).

In the ^{15}N -photo-CIDNP MAS NMR spectrum of *Cab. thermophilum*, the strongest signal is observed at 216.0 ppm. In comparison to the three (B)Chls found in *Cab. thermophilum*, this very characteristic signal matches best to the N-II of Chl *a* at 206.0 ppm. The resonance at 250.1 ppm can conveniently be assigned to N-IV and the signal at 191.4 ppm corresponds to N-III. Hence, we conclude that the three ^{15}N photo-CIDNP MAS NMR signals that are observed in membranes of *Cab. thermophilum* originate from Chl *a*, although the signals appear slightly disturbed, especially at ring II. A comparison to the signals observed in the other three RCs, however, reveals that the N-II resonance differs by only a few ppm. Hence, the chemical shifts of the three ^{15}N signals reported here match well to those of Chl *a* incorporated in other RCs.

The question now arises whether Chl *a* acts as the donor or the acceptor within the spin-correlated radical pair. The RC complex of *Cab. thermophilum* contains three pigments in the ratio 1.6 Zn-BChl *a'*, 10.3 Chl *a*, and 6.4 BChl *a* molecules per P840 donor. The light-induced optical difference spectrum (P^+ minus P) exhibits maximal photobleaching near 840 nm, which indicates that Chl *a* is certainly not the primary donor for these RCs. There are probably at least two Zn-BChl *a'* molecules in the RC, implying that these two molecules could form a dimeric donor in the electron transfer cofactor chain. All known type-1 RCs have at least one epimer form of (B)Chl as the electron donor. For example, heliobacterial RCs contain two BChl *g'* molecules as the symmetric dimeric donor, and these RCs further contain two BChl *g'* molecules within the core antenna portion of the RC (Gisriel et al. 2017). These observations strongly suggest that Zn-BChl *a'* acts as the electron donor in *Cab. thermophilum*. This implies that the observed Chl *a* portion of the spin-correlated radical pair acts as the electron acceptor. The spin-correlated radical pair would therefore be formed by Zn-BChl *a'* as the donor and Chl *a* as the acceptor. The occurrence of a single set of signals from the acceptor can be interpreted to indicate that either only one branch of cofactors is active, or that both branches are active and contain identical acceptor cofactors. Because the RC is a homodimer of PscA subunits (Tsukatani et al. 2012), the results are consistent with the latter option of a symmetric dimer. The absence of signals from the donor in this photo-CIDNP MAS NMR experiment might be an experimental accident because of the field strength chosen. It might be that the positive (enhanced absorptive) contributions by the DD and DR mechanisms cancel the negative (emissive) contributions by the TSM mechanism.

A comparison of the ^{15}N -photo-CIDNP MAS NMR spectrum of Chl *a* to those of other species reveals a high similarity to PS I from plants (Diller et al. 2007a) and diatoms

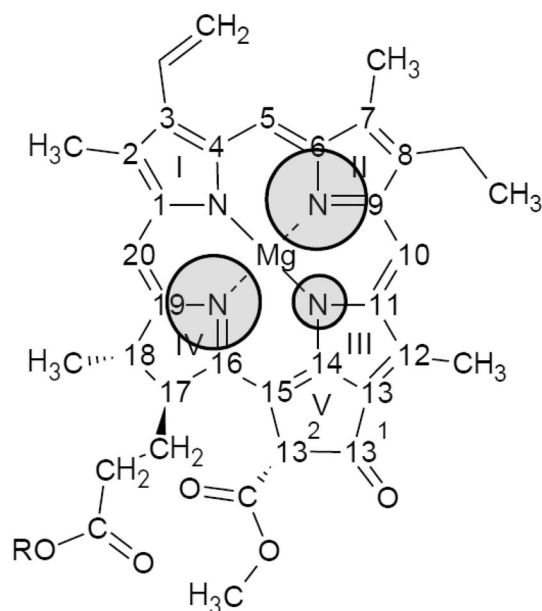


Fig. 5 ^{15}N photo-CIDNP MAS NMR intensity pattern of *Cab. thermophilum*

(Zill 2017a). *Cba. tepidum* from the phylum *Chlorobi* also utilizes Chl *a* as electron acceptor (Roy et al. 2007a). Furthermore, in the RCs of heliobacteria, $8^1\text{-OH Chl } a$ acts as primary electron acceptor (Thamarath et al. 2012; Gisriel et al. 2017). The type-1 RCs from *H. mobilis* only showed signals induced by the donor for the anaerobic Braunstoff preparation and predominantly resonances from the acceptor in case of the aerobic Grünstoff (Thamarath et al. 2012). Comparison of ^{15}N -photo-CIDNP MAS NMR spectra from *Cab. thermophilum* and the aerobic RCs from *H. mobilis* also reveals good matching. As we have seen above, ^{15}N NMR is unable to distinguish Chl *a* and $8^1\text{-OH Chl } a$, in the present case; however, only because Chl *a* is present and $8^1\text{-OH Chl } a$ can be excluded biochemically, we conclude that the primary acceptor must be Chl *a*.

All ^{15}N photo-CIDNP MAS NMR signals (Figs. 4 and S5) appear with emissive sign, which can be explained by a predominance of the TSM over the DD mechanism. The DR mechanism does not contribute to signals from the acceptor. The lineshape of the observed signals is Lorentzian, indicating that the natural lineshape remains undisturbed. The strongest signal at 216.0 ppm is slightly broader (full width half maximum = FWHM of 70 Hz) than the signal at 250.1 ppm (FWHM of 48 Hz). The narrow linewidth is typical for photosynthetic RCs and is explained by a rigid inner part of the RC (Fischer et al. 1992; Diller et al. 2007a).

Figure 5 shows the photo-CIDNP intensity pattern of Chl *a*, which acts most likely as the primary electron acceptor in *Cab. thermophilum*. The depicted signal intensities correlate to the local electron spin densities at this position (Diller

et al. 2007b). As in plant PS I (Diller et al. 2007a) and Grünstoff of heliobacteria (Thamarath et al. 2012), N-II shows the highest intensity.

Conclusions

The solid-state photo-CIDNP effect is observed in the membranes of *Cab. thermophilum* by ^{15}N -MAS NMR. This is the first time that the effect has been found in RCs of an organism from the phylum *Acidobacteria*. The high number of species as well as the large variety of taxonomic ranks indicates that the effect is an intrinsic property of all photosynthetic species and their RCs. Hence, photosynthetic functionalities appear to be exceptionally constant on very long evolutionary timescales. The results suggest that details concerning the mechanism of primary charge separation are conserved in all types of RCs, which may indicate that primary charge separation in RCs occurs by a single, physically similar process in all RCs. This finding is in general agreement with the widely accepted idea that photochemical reaction centers evolved once and subsequently diversified by processes including gene duplication, divergence, and horizontal gene transfer (e.g., see recent reviews by Cardona 2015; Fischer et al. 2016; Martin et al. 2018).

A set of three ^{15}N NMR signals is observed in the photo-CIDNP MAS NMR spectrum of the type-1 homodimeric RCs of *Cab. thermophilum*. To identify the cofactor observed with photo-CIDNP MAS NMR, ^{15}N -chemical shifts of Zn-BChl *a* were determined from solution-state NMR experiments as well as from calculations. The chemical shifts of Zn-BChl *a* as well as values of Mg-BChl *a* known from literature do not match the resonances observed with ^{15}N -photo-CIDNP MAS NMR. The photo-CIDNP signals, however, match well to the chemical shifts of Chl *a*. We conclude that Chl *a* acts as primary electron acceptor, implying that Zn-BChl *a'* is the electron donor in these RCs. The absence of signal splitting is consistent with the observed acceptor cofactor being a part of a symmetrical electron transport chain in this homodimeric RC.

Acknowledgements The authors thank Dr. Matthias Findeisen for technical assistance, Eva-Maria Höhn (Group of Professor Dr. Detlev Belder, Universität Leipzig) for the Raman measurements, and Prof. Dr. Stefan Berger (Leipzig) for discussions. J.M. acknowledges the generous support of the Deutsche Forschungsgemeinschaft DFG (MA4972/2-1). Studies in the laboratories of D.A.B. and J.H.G. were supported by Grants DE-FG02-94ER20137 and DE-SC0010575, respectively, from the Photosynthetic Systems Program, Division of Chemical Sciences, Geosciences, and Biosciences (CSGB), Office of Basic Energy Sciences of the U. S. Department of Energy. I.S. is supported by the ERC Starting Grant ‘PhotoMutant’ (678169). Y.L. would like to thank Dr. Dror Noy (MIGAL) and his financial support from the ERC (GA 615217) and ISF (GA 558/14).

References

- Alia A, Roy E, Gast P et al (2004) Photochemically induced dynamic nuclear polarization in photosystem I of plants observed by ^{13}C magic-angle spinning NMR. *J Am Chem Soc* 126:12819–12826. <https://doi.org/10.1021/ja048051+>
- Becke AD (1993) Density-functional thermochemistry. III. The role of exact exchange. *J Chem Phys* 98:5648–5652. <https://doi.org/10.1063/1.464913>
- Bennett AE, Rienstra CM, Auger M et al (1995) Heteronuclear decoupling in rotating solids. *J Chem Phys* 103:6951–6958. <https://doi.org/10.1063/1.470372>
- Bode B, Thamarath SS, Sai Sankar Gupta KB, Alia A, Jeschke G, Matysik J (2013) The solid-state photo-CIDNP effect and its analytical application. In: Kuhn L (ed) *Hyperpolarization methods in NMR spectroscopy*. Springer, Berlin, pp 105–121
- Boxer SG, Closs GL, Katz JJ (1974) The effect of magnesium coordination on the ^{13}C and ^{15}N magnetic resonance spectra of chlorophyll *a*. Energies of nitrogen n_{π}^* states as deduced from a the relative complete assignment of chemical shifts. *J Am Chem Soc* 96:7058–7066. <https://doi.org/10.1021/ja00829a038>
- Bryant DA, Frigaard NU (2006) Prokaryotic photosynthesis and phototrophy illuminated. *Trends Microbiol* 14:488–496. <https://doi.org/10.1016/j.tim.2006.09.001>
- Bryant DA, Garcia Costas AM, Maresca JA et al (2007) *Candidatus Chloracidobacterium thermophilum*: an aerobic phototrophic acidobacterium. *Science* 317:523–526. <https://doi.org/10.1126/science.1143236>
- Cardona T (2015) A fresh look at the evolution and diversification of photochemical reaction centers. *Photosynth Res* 126:111–134. <https://doi.org/10.1007/s11120-014-0065-x>
- Cavalier-Smith T (1998) A revised six-kingdom system of life. *Biol Rev* 73:203–266
- Céspedes-Camacho IF, Matysik J (2014) Spin in photosynthetic electron transport. In: Golbeck J, van der Est A (eds) *The biophysics of photosynthesis*. Springer, New York, pp 141–170
- Chen GE, Canniffe DP, Martin EC, Hunter CN (2016) Absence of the *cbh*₃ terminal oxidase reveals an active oxygen-dependent cyclase involved in bacteriochlorophyll biosynthesis in *Rhodobacter sphaeroides*. *J Bacteriol* 198:2056–2063. <https://doi.org/10.1128/JB.00121-16>
- Daviso E, Jeschke G, Matysik J (2008a) Photochemically induced dynamic nuclear polarization (photo-CIDNP) magic-angle spinning NMR. In: Aartsma TJ, Matysik J (eds) *Biophysical techniques in photosynthesis*. Springer, Dordrecht, pp 385–399
- Daviso E, Gupta KBSS, Prakash S et al (2008b) ^{15}N photo-CIDNP MAS NMR on RCs of *Rhodobacter sphaeroides* WT and R26. In: Allen JF, Gantt E, Golbeck JH, Osmond B (eds) *Energy from the sun*. Springer, Dordrecht, pp 25–28
- Diller A, Alia A, Roy E et al (2005) Photo-CIDNP solid-state NMR on photosystems I and II: what makes P680 special? *Photosynth Res* 84:303–308. <https://doi.org/10.1007/s11120-005-0411-0>
- Diller A, Roy E, Gast P et al (2007a) ^{15}N photochemically induced dynamic nuclear polarization magic-angle spinning NMR analysis of the electron donor of photosystem II. *Proc Natl Acad Sci USA* 104:12767–12771. <https://doi.org/10.1073/pnas.0701763104>
- Diller A, Prakash S, Alia A, Gast P, Matysik J, Jeschke G (2007b) Signals in solid-state photochemically induced dynamic nuclear polarization recover faster than with the longitudinal relaxation time. *J Phys Chem B* 111:10606–10614. <https://doi.org/10.1021/jp072428r>
- Diller A, Alia A, Gast P et al (2008) ^{13}C photo-CIDNP MAS NMR on the LH1-RC complex of *Rhodospseudomonas acidophila*. In: Allen JF, Gantt E, Golbeck JH, Osmond B (eds) *Energy from the sun*. Springer, Dordrecht, pp 55–58
- Egorova-Zachernyuk T, van Rossum B, Erkelens C, de Groot H (2008) Characterisation of uniformly ^{13}C , ^{15}N labelled bacteriochlorophyll *a* and bacteriopheophytin *a* in solution and in solid state: complete assignment of the ^{13}C , ^1H and ^{15}N chemical shifts. *Magn Res Chem* 46:1074–1083. <https://doi.org/10.1002/mr3c.2295>
- Fischer MR, de Groot HJM, Raap J et al (1992) ^{13}C Magic angle spinning NMR study of the light-induced and temperature-dependent changes in *Rhodobacter sphaeroides* R26 reaction centers enriched in [4'- ^{13}C]tyrosine. *Biochemistry* 31:11038–11049
- Fischer WW, Hemp J, Johnson JE (2016) Evolution of oxygenic photosynthesis. *Annu Rev Earth Planet Sci* 44:647–683. <https://doi.org/10.1146/annurev-earth-060313-054810>
- Frisch MJ, Trucks GW, Schlegel HB et al (2009) Gaussian 09, revision D. 01. Gaussian Inc., Wallingford
- Gisriel C, Sarrou I, Ferlez B et al (2017) Structure of a symmetric photosynthetic reaction center-photosystem. *Science* 357:1021–1025. <https://doi.org/10.1126/science.aan5611>
- Golbeck JH (2003) Shared thematic elements in photochemical reaction centers. *Proc Natl Acad Sci USA* 90:1642–1646. <https://doi.org/10.1073/pnas.90.5.1642>
- Grimme S, Ehrlich S, Goerigk L (2011) Effect of the damping function in dispersion corrected density functional theory. *J Comput Chem* 32:1456–1465. <https://doi.org/10.1002/jcc.21759>
- Janssen GJ, Daviso E, van Son M et al (2010) Observation of the solid-state photo-CIDNP effect in entire cells of cyanobacteria *Synechocystis*. *Photosynth Res* 104:275–282. <https://doi.org/10.1007/s11120-009-9508-1>
- Janssen GJ, Roy E, Matysik J, Alia A (2012) ^{15}N photo-CIDNP MAS NMR to reveal functional heterogeneity in electron donor of different plant organisms. *Appl Magn Reson* 42:57–67. <https://doi.org/10.1007/s00723-011-0283-8>
- Jeschke G (1998) A new mechanism for chemically induced dynamic nuclear polarization in the solid state. *J Am Chem Soc* 120:4425–4429. <https://doi.org/10.1021/ja973744u>
- Jeschke G, Matysik J (2003) A reassessment of the origin of photochemically induced dynamic nuclear polarization effects in solids. *Chem Phys* 294:239–255. [https://doi.org/10.1016/S0301-0104\(03\)00278-7](https://doi.org/10.1016/S0301-0104(03)00278-7)
- Kobayashi M, Akiyama M, Yamamura M et al (1998) Structural determination of the novel Zn-containing bacteriochlorophyll in *Acidiphilium rubrum*. *Photomed Photobiol* 20:75–80
- Kobayashi M, Akiyama M, Kano H, Kise H (2006) Spectroscopy and structure determination. In: Govindjee, Sharkey TD (eds) *Advances in photosynthesis and respiration*, vol 25. Chlorophylls and bacteriochlorophylls: biochemistry, biophysics, function and applications. Springer, Dordrecht, pp 79–94
- Kobayashi M, Sorimachi Y, Fukayama D et al (2016) Physicochemical properties of chlorophylls and bacteriochlorophylls. In: Pessarakki M (ed) *Handbook of photosynthesis*. CRC Press, Boca Raton, pp 95–148
- Li H, Jubelirer S, Garcia Costas AM et al (2009) Multiple antioxidant proteins protect *Chlorobaculum tepidum* against oxygen and reactive oxygen species. *Arch Microbiol* 191:853–867. <https://doi.org/10.1007/s00203-009-0514-7>
- Liu Z, Klatt CG, Ludwig M, Rusch DB, Jensen SI, Kühl M, Ward DM, Bryant DA (2012) '*Candidatus Thermochlorobacter aerophilum*': an aerobic chlorophotoheterotrophic member of the phylum *Chlorobi*. *ISME J* 6:1869–1882
- Madigan MT (2001) Firmicutes. In: Whitman W (ed) *Bergey's manual of systematic bacteriology*. Springer, New York, pp 625–630
- Marenich AV, Cramer CJ, Truhlar DG (2009) Performance of SM6, SM8, and SMD on the SAMPL1 test set for the prediction of small-molecule solvation free energies. *J Phys Chem B* 113:6378–6396. <https://doi.org/10.1021/jp809094y>

- Martin WF, Beatty JT, Bryant DA (2018) A physiological perspective on the origin and evolution of photosynthesis. *FEMS Microbiol Rev* 42:205–231. <https://doi.org/10.1093/femsre/fux056>
- Matysik J, Alia A, Hollander JG et al (2000) A set-up to study photochemically induced dynamic nuclear polarization in photosynthetic reaction centres by solid-state NMR. *Indian J Biochem Biophys* 37:418
- Matysik J, Diller A, Roy E, Alia A (2009) The solid-state photo-CIDNP effect. *Photosynth Res* 102:427–435. <https://doi.org/10.1007/s11120-009-9403-9>
- McDermott A, Zysmilich MG, Polenova T (1998) Solid state NMR studies of photoinduced polarization in photosynthetic reaction centers: mechanism and simulations. *Solid State Nucl Magn Reson* 11:21–47. [https://doi.org/10.1016/S0926-2040\(97\)00094-5](https://doi.org/10.1016/S0926-2040(97)00094-5)
- Oh-oka H (2007) Type 1 reaction center of photosynthetic heliobacteria. *Photochem Photobiol* 83:177–186. <https://doi.org/10.1562/2006-03-29-IR-860>
- Overmann J (2001) Chlorobi. In: Boone DR, Castenholz RW (eds) *Bergey's manual of systematic bacteriology*. Springer, New York, pp 601–605
- Polenova T, McDermott AE (1999) A coherent mixing mechanism explains the photoinduced nuclear polarization in photosynthetic reaction centers. *J Phys Chem* 103:535–548. <https://doi.org/10.1021/jp9822642>
- Prakash S, Alia A, Gast P, de Groot HJM, Jeschke G, Matysik J (2005) Magnetic field dependence of photo-CIDNP MAS NMR on photosynthetic reaction centres of *Rhodobacter sphaeroides* WT. *J Am Chem Soc* 127:14290–14298. <https://doi.org/10.1021/ja0623616>
- Prakash S, Alia A, Gast P et al (2006) Photo-CIDNP MAS NMR in intact cells of *Rhodobacter sphaeroides* R26: molecular and atomic resolution at nanomolar concentration. *J Am Chem Soc* 128:12794–12799. <https://doi.org/10.1021/ja0623616>
- Rassolov VA, Ratner MA, Pople JA et al (2001) 6-31G* basis set for third-row atoms. *J Comput Chem* 22:976–984. <https://doi.org/10.1002/jcc.1058>
- Roy E, Alia A, Gast P et al (2007a) Photochemically induced dynamic nuclear polarization in the reaction center of the green sulphur bacterium *Chlorobium tepidum* observed by ^{13}C MAS NMR. *Biochim Biophys Acta* 1767:610–615. <https://doi.org/10.1016/j.bbabi.2006.12.012>
- Roy E, Diller A, Alia A et al (2007b) Magnetic field dependence of ^{13}C photo-CIDNP MAS NMR in plant photosystems I and II. *Appl Magn Reson* 31:193–204. <https://doi.org/10.1007/BF03166256>
- Roy E, Rohmer T, Gast P et al (2008) Characterization of the primary radical pair in reaction centers of *Heliobacillus mobilis* by ^{13}C photo-CIDNP MAS NMR. *Biochemistry* 47:4629–4635. <https://doi.org/10.1021/bi800030g>
- Ruud K, Helgaker T, Bak KL et al (1993) Hartree–Fock limit magnetizabilities from London orbitals. *J Chem Phys* 99:3847–3859. <https://doi.org/10.1063/1.466131>
- Schulten EAM, Matysik J, Alia A et al (2002) ^{13}C MAS NMR and photo-CIDNP reveal a pronounced asymmetry in the electronic ground state of the special pair of *Rhodobacter sphaeroides* reaction centers. *Biochemistry* 41:8708–8717. <https://doi.org/10.1021/bi025608u>
- Sosnovsky DV, Jeschke G, Matysik J, Vieth H-M, Ivanov KL (2016) Level crossing analysis of chemically induced dynamic nuclear polarization: towards a common description of liquid-state and solid-state cases. *J Chem Phys* 144:144202. <https://doi.org/10.1063/1.4945341>
- Tank M, Bryant DA (2015a) *Chloracidobacterium thermophilum* gen. nov., sp. nov.: an anoxygenic microaerophilic chlorophotoheterotrophic acidobacterium. *Int J Syst Evol Microbiol* 65:1426–1430. <https://doi.org/10.1099/ijs.0.000113>
- Tank M, Bryant DA (2015b) Nutrient requirements and growth physiology of the photoheterotrophic acidobacterium, *Chloracidobacterium thermophilum*. *Front Microbiol* 6:226. <https://doi.org/10.3389/fmicb.2015.00226>
- Tank M, Thiel V, Bryant DA (2017) A panoply of phototrophs: an overview of chlorophototrophs found in the microbial mats of alkaline siliceous hot springs in Yellowstone National Park, WY, USA. In: Hallenbeck PC (ed) *Modern topics in the phototrophic prokaryotes: environmental and applied aspects*. Springer, Berlin, pp 87–137. <https://doi.org/10.1007/978-3-319-46261-5>
- Thamarath SS, Heberle J, Hore P et al (2010) Solid-state photo-CIDNP effect observed in phototropin LOV1-C57S by ^{13}C magic-angle spinning NMR spectroscopy. *J Am Chem Soc* 132:15542–15543. <https://doi.org/10.1021/ja1082969>
- Thamarath SS, Alia A, Daviso E et al (2012) Whole cell nuclear magnetic resonance characterization of two photochemically active states of the photosynthetic reaction center in heliobacteria. *Biochemistry* 51:5763–5773. <https://doi.org/10.1021/bi300468y>
- Thiel V, Tank M, Bryant DA (2017) Diversity of chlorophototrophic bacteria revealed in the omics era. *Annu Rev Plant Biol*. <https://doi.org/10.1146/annurev-arplant-042817-040500>
- Tsukatani Y, Romberger SP, Golbeck JH, Bryant DA (2012) Isolation and characterization of homodimeric type-I reaction center complex from Candidatus *Chloracidobacterium thermophilum*, an aerobic chlorophototroph. *J Biol Chem* 287:5720–5732. <https://doi.org/10.1074/jbc.M111.323329>
- van Heukelem L, Lewitus AJ, Kana TM, Craft NE (1994) Improved separations of phytoplankton pigments using temperature-controlled high performance liquid chromatography. *Mar Ecol Prog Ser* 114:304–313
- Wakao N, Yokoi N, Isoyama N et al (1996) Discovery of natural photosynthesis using Zn-containing bacteriochlorophyll in an aerobic bacterium *Acidiphilium rubrum*. *Plant cell Physiol* 37:889–893. <https://doi.org/10.1093/oxfordjournals.pcp.a0290293>
- Wen J, Tsukatani Y, Cui W, Zhang H, Gross ML, Bryant DA, Blankenship RE (2011) Structural model and spectroscopic characteristics of the FMO antenna protein from the aerobic chlorophototroph, Candidatus *Chloracidobacterium thermophilum*. *Biochim Biophys Acta* 1807:157–164. <https://doi.org/10.1016/j.bbabi.2010.09.008>
- Zeng Y, Feng F, Medová H et al (2014) Functional type 2 photosynthetic reaction centers found in the rare bacterial phylum *Gemmatimonadetes*. *Proc Natl Acad Sci USA* 111:7795–7800. <https://doi.org/10.1073/pnas.1400295111>
- Zill JC (2017a) Der Festkörper photo-CIDNP-Effekt im Baum des Lebens, Dissertation, Universität Leipzig
- Zill JC, Kansy M, Goss R et al (2017b) Photo-CIDNP in the reaction center of the drom *Cyclotella meneghiniana* observed by ^{13}C MAS NMR. *Z Phys Chem* 231:347–367. <https://doi.org/10.1515/zpch-2016-0806>
- Zysmilich MG, McDermott A (1994) Photochemically induced dynamic nuclear polarization in the solid-state ^{15}N spectra of reaction centers from photosynthetic bacteria *Rhodobacter sphaeroides* R-26. *J Am Chem Soc* 116:8362–8363. <https://doi.org/10.1021/ja00097a052>